Early detection of fatigue damage processes by infrared investigation of thermomechanical coupling phenomena

Justus Medgenberg[a], Thomas Ummenhofer[a]

[a] Institut fuer Bauwerkserhaltung und Tragwerk
Technische Universitaet Carolo-Wilhelmina, 38106 Braunschweig, Germany

Abstract The following paper presents a new experimental approach for the analysis of localized fatigue damage phenomena based on infrared thermography. First the effect of different thermomechanical coupling phenomena on the surface temperature evolution during mechanical harmonic loading is discussed based on numerical simulations. These findings propose the application of a specialized methodology for experimental investigations, which allows for the in-situ analysis of typical fatigue processes as cyclic plasticity and crack initiation. The presented technique is based on the measurement of thermomechanical coupling phenomena by high-resolution infrared thermography and specialized data processing. In contrast to other well-known approaches using thermal measurements the short term temperature evolution during mechanical loading is analyzed locally. This offers a very high spatial resolution and allows for the analysis of extremely localized damage phenomena. The approach has been successfully applied during fatigue testing of different welded as well as un-welded notched and un-notched specimens. The application of the thermal measurements is non-contacting, fast and does not require interruptions of the testing. The experimental results confirm that damage-relevant phenomena as cyclic plasticity and crack initiation can be resolved and analyzed.

1 INTRODUCTION

A special issue of fatigue testing is the investigation and identification of continuous damage processes. Typically the assessment of the fatigue damage process is based on conventional measurement techniques as strain gauges, monitoring of the forces or displacements of the testing machine, wire-based crack detectors, penetration tests, visual inspection by eye or digital cameras, acoustic emission etc. The mayor disadvantages of the existing techniques are:

- They fail to resolve and localize the strongly heterogeneously distributed early damage processes (strain gauge measurements, force and displacement monitoring)
- They require a pre-knowledge on potential hot spots and a rather time-consuming preparation of the specimens in these points (strain gauges, wire crack detectors)
- They can not be applied online (visual inspection by eye, penetration test)
- The calibration of the methods and the relation to the underlying damage processes is difficult and involves uncertainties (acoustic emission)

The listed disadvantages contribute to the fact that termination criteria for fatigue testing are not unique and often lack of a strict physical basis. As an alternative tool non-destructive inspection techniques based on infrared thermography have been proposed recently. Due to the rapid advances in infrared technology and falling costs for high resolution infrared cameras the application of thermography as a regular inspection technique during mechanical testing becomes interesting. The idea behind the application is the investigation of thermomechanical coupling phenomena and their analysis with respect to damage processes. The advantages are easy applicability without extensive specimen preparation, full-field resolution and a clear physical meaning of the observed temperature changes. Even though the recording of the temperature changes during mechanical loading is relatively easy, the post-processing and interpretation of the data requires in-depth knowledge of the underlying processes. High spatial resolution can be obtained by investigating the short time fluctuations of the temperature around the equilibrium state rather than focusing on the analysis of the mean temperature evolution. Potential information obtainable by thermal inspection techniques is:

- stress concentrations
- distinction between elastic material behaviour and cyclic plasticity
- crack initiation and crack growth

Thus thermal inspection allows for the detection of the most relevant parameters for the fatigue process which yields an enormous and so far mostly unused potential for the application of thermography during fatigue loading. In the stage reported here we focus on qualitative rather than quantitative measurements.

2 THERMOMECHANICAL BACKGROUND

The heat equation of a deformable solid body with thermoelastic coupling and thermoplastic dissipation can be derived from the first and second principle of thermodynamics. In case of no additional external or internal heat sources it can be written as [1]

$$\rho C_{\varepsilon} \frac{dT}{dt} - \frac{\partial}{\partial x_j} k \left(\frac{\partial T}{\partial x_j} \right) = T \frac{\partial \sigma_{ij}}{\partial T} \frac{d\varepsilon^e_{ij}}{dt} + \sigma_{ij} \frac{d\varepsilon^p_{ij}}{dt} - a \frac{d\varepsilon^p_{ij}}{dt} \tag{1}$$

In equation (1) ρ is the density, C_ε is the heat capacity at constant strain, T is the temperature, k is the heat conductivity tensor, σ_{ij} is the symmetric Cauchy stress tensor, ε_{ij}^e is the reversible (elastic) part of the strain tensor and ε_{ij}^p is the irreversible (plastic) part of the strain tensor. For the derivation an additive decomposition of the total strain tensor into an elastic and a plastic part has been used. The last term on the right hand side depending on ε_{ij}^p is the intrinsic dissipation given as the sum of the plastic dissipation plus the evolution of the internal hardening state. Further coupling phenomena as thermoplastic coupling or the dependency of any material coefficients on the hardening state have been neglected in this stage. The dimensionless coefficient a represents the portion of the total dissipation which is stored in form of irreversible changes of the internal material structure. Generally the ratio of the intrinsic dissipation to the plastic work is close to 1.0 [4]. At this point we assume that the entire plastic dissipation is released as heat so that $a=0$. For isotropic materials as metals the heat conductivity tensor is replaced by the constant coefficient of heat conduction.

The first term on the right hand side is the thermoelastic coupling term. Based on Hooke's law one has

$$\sigma_{ij} = \frac{E}{1+\upsilon} \varepsilon_{ij} + \left[\frac{E\upsilon}{(1+\upsilon)(1-2\upsilon)} \varepsilon_I^e - \frac{E}{1-2\upsilon} \alpha \Delta T \right] \delta_{ij} \tag{2}$$

In equation (2) E is the Young's modulus, υ the Poisson's ratio, α is the coefficient of thermal expansion and δ_{ij} is Kronecker's delta with $\delta_{ij}=1$ if i = j and $\delta_{ij}=0$ if i ≠ j. ε^e_I represents the first invariant of the elastic strain tensor $\varepsilon^e_I=\varepsilon^e_{11}+\varepsilon^e_{22}+\varepsilon^e_{33}$. The differentiation of (2) with respect to temperature is given as

$$\frac{\partial \sigma_{ij}}{\partial T} = \left[\frac{1}{1+\upsilon} \frac{\partial E}{\partial T} - \frac{E}{(1+\upsilon)^2} \frac{\partial \upsilon}{\partial T} \right] \varepsilon^e_{ij} + \left[\left(\frac{\upsilon}{(1+\upsilon)(1-2\upsilon)} \frac{\partial E}{\partial T} + \frac{E(2\upsilon^2+1)}{(1+\upsilon)^2(1-2\upsilon)^2} \frac{\partial \upsilon}{\partial T} \right) \varepsilon^e_I - \frac{E\alpha}{1-2\upsilon} \right] \delta_{ij} \tag{3}$$

which can be plugged into the thermoelastic coupling term of equation (1). Note that for the derivation of (3) the temperature dependency of the Young's modulus and the Poisson's ratio has been taken into account. This approach corresponds to the extended theory of thermoelasticity presented by [10].

3 NUMERICAL INVESTIGATIONS

3.1 Approach

Equation (1) together with the elastic material model given by (3) constitutes the basis for the analysis of the temperature changes induced by mechanical loading of a solid body. A numerical solution of (1) can be obtained for an arbitrary geometry by means of a commercial FE-Program (ANSYS R10) and is based on the subsequent solution of a mechanical and a thermal model [8]. The mechanical model solves for the stresses and strains due to arbitrary mechanical loading. Next the local values of the coupling term (3) and the plastic work term in equation (1) are calculated based on the mechanical results and transferred as equivalent heat sources to a transient thermal model which solves the left hand side of (1) for the temperature field. The procedure is repeated for every time step. Bidirectional coupling, i.e. the effect of the temperature changes on the stresses and strains can be considered by transferring the calculated temperature field back as thermal loads onto the mechanical model. Depending on the focus of the investigations individual effects as the thermal dependence of the Young's modulus and/or the Poisson's ratio, plasticity, bidirectional coupling etc. can or can not be incorporated for the calculation. As a test case we use the cylindrical specimen type shown in figure 1 a). All investigations refer to mild carbon steel S355J2G3 whose material parameters have been specified and are summarized in table I. Harmonic force-controlled loading acting in the longitudinal direction of the specimen is applied to the upper and lower end of the specimen which corresponds to the situation during the experimental fatigue tests discussed later on. The loading frequency f_L varies between 2.5 Hz and 15 Hz, depending on the purpose of the investigations.

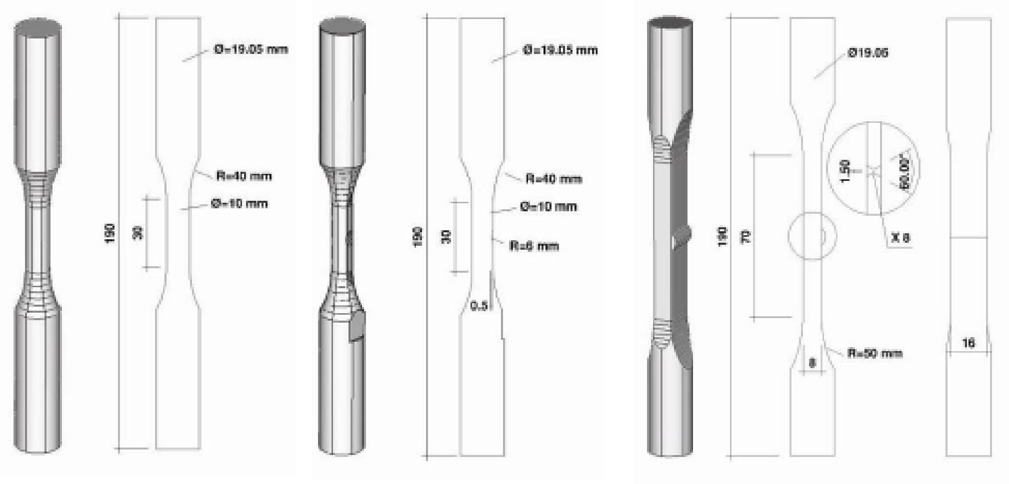

a) cylindrical specimen *b) notched specimen* *c) welded specimen*

Figure 1. Specimen geometries used for numerical and experimental studies.

Table I. Material properties for the used mild steel S355J2G3.

ρ [kg/m³] 7830	c_ε [J/(kg·K)] 429	k [W/(m·K)] 42	α [1/K] $8.8\cdot10^{-6}$	$\partial E/\partial T$ [MPa/K] -76.6	$\partial \upsilon/\partial T$ [1/K] ≈ 0
$\sigma_{y,l}$ [MPa] 352	$\sigma_{y,u}$ [MPa] 464	σ_u [MPa] 546	σ_{y0} [MPa] ≈ 210	E [MPa] 214300	

3.2 Influence of cyclic plasticity

In order to simulate the cyclic material behaviour of the steel a multi-linear plasticity model based on a Besseling sub-layer model has been adjusted to measured stabilized stress-strain hysteresis loops. The plasticity model is readily implemented in ANSYS R10 and can be used to model complex elastic-plastic materials. The initial yield limit σ_{y0} of the model has been set to the experimentally determined cyclic yield limit of 210 MPa. Based on the numerical results for the stresses and the elastic and plastic strains the values of the coupling terms on the right hand side of equation (1) are evaluated for each time step. Generally the time step size is set to 1/40 of a load cycle which has been found to be a good trade-off between the accuracy of the results and computational effort. The temperature dependency of the Young's modulus and the Poisson's ratio is neglected at this point. Figure 2 a) shows the temporal evolution of the thermoelastic coupling term for an elastic-plastic and a corresponding linear elastic model under the same loading conditions. Figure 2 b) shows the difference of the coupling term between both models. Figure 2 c) gives the corresponding plastic work rate of the elastic-plastic model and the temperature evolution of both models. The results refer to a single point on the surface of the cylindrical specimen under harmonic loading with a load amplitude of 21 kN and a loading frequency of 2.5 Hz. According to the numerical results the elastic work rate is not influenced by the occurrence of plastic deformations which means that the thermoelastic coupling remains unchanged. For harmonic loading the thermoelastic temperature changes thus remain harmonic even in case of plastic deformations.

Figure 2 c) shows that the plastic work rate becomes nonzero if the yield limit is exceeded. In contrast to the thermoelastic coupling it always remains positive and thus leads to a rise of the mean temperature of the specimen. Figure 3 gives the temperature difference between the elastic-plastic and a corresponding purely elastic solution prior and after removal of the trend due to the increase of the mean temperature. Figure 3 b) demonstrates that the onset of plastic deformations is marked by characteristic nonlinearities in the temperature evolution which will in the following be used to analyze the temperature signals for damage relevant processes. The linear and nonlinear temperature signals are represented from now on by their amplitude values T_a^{lin} and T_a^{nlin}, respectively. Obviously the temperature changes caused by plastic dissipation are non-harmonic. Their fundamental frequency equals $2\cdot f_L$ but they also bear higher frequency contributions.

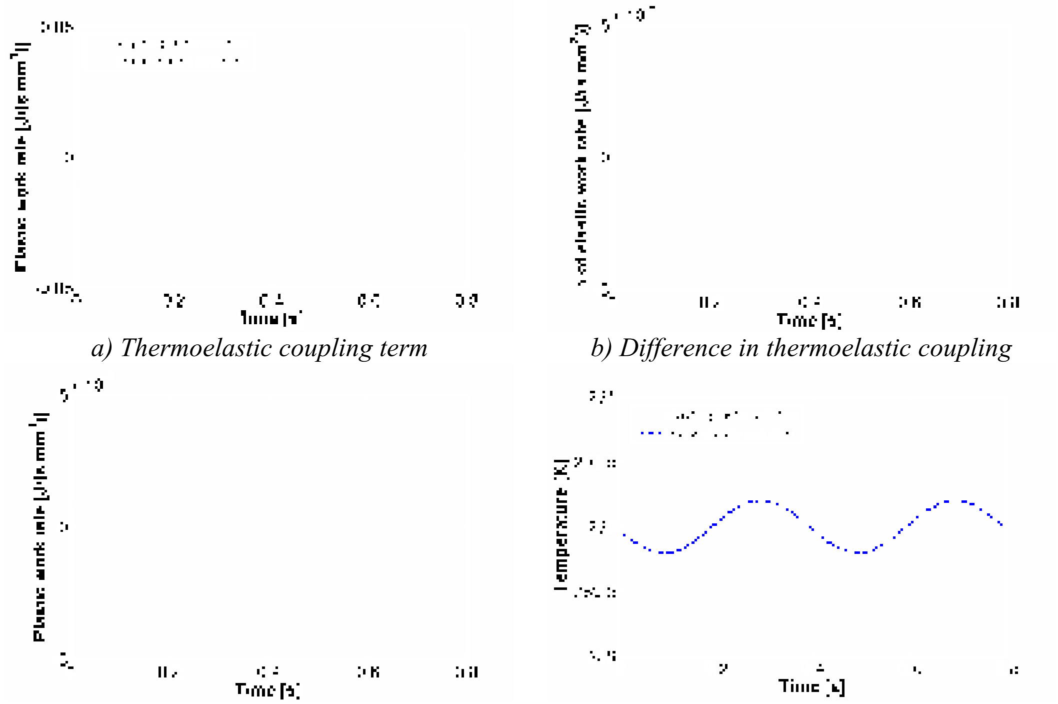

a) Thermoelastic coupling term *b) Difference in thermoelastic coupling*

c) Plastic work rate *d) Temperature evolution*

Figure 2. Effect of elastic-plastic material behaviour on the thermomechanical coupling, F_a=21 kN, f_L=2.5 Hz.

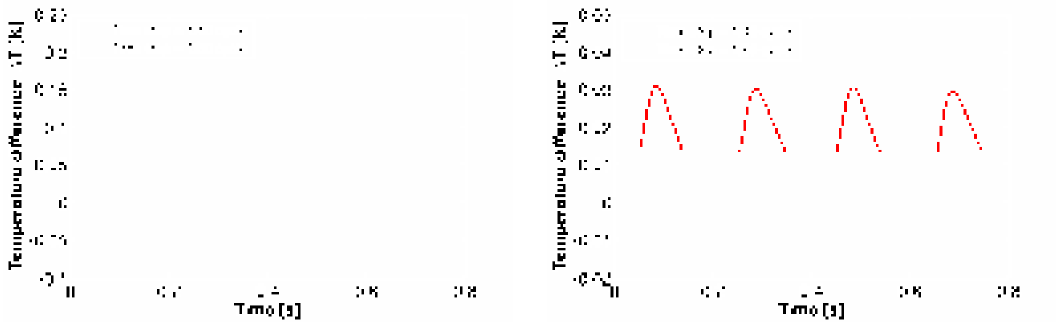

a) with trend *a) without trend*

Figure 3. Temperature difference between elastic-plastic and linear-elastic material behaviour, F_a=21 kN, f_L=2.5 Hz.

3.3 Influence of mean loads

The influence of means loads on the thermoelastic coupling has first been observed experimentally by [5] and can be explained by the temperature dependency of the Young's modulus. If the temperature dependency of the Poisson's ratio is omitted in equation (3) one gets the three thermoelastic coupling terms:

$$\textit{Term I:} \quad T\left(-\frac{E\alpha}{1-2\upsilon}\right)\dot{\varepsilon}_I^e \tag{4}$$

$$\textit{Term II:} \quad T\left(\frac{1}{1+\upsilon}\frac{\partial E}{\partial T}\right)\left(\varepsilon_{11}^e\dot{\varepsilon}_{11}^e+\varepsilon_{22}^e\dot{\varepsilon}_{22}^e+\varepsilon_{33}^e\dot{\varepsilon}_{33}^e\right) \tag{5}$$

$$\textit{Term III:} \quad T\left(\frac{\upsilon}{(1+\upsilon)(1-2\upsilon)}\frac{\partial E}{\partial T}\right)\varepsilon_I^e\dot{\varepsilon}_I^e \tag{6}$$

Term I represents the classical thermoelastic coupling and depends on the load amplitude only. Terms II through III arise due to the temperature dependency of the Young's modulus and cause a higher order dependency on the load amplitude and the mean load level. The temperature T which appears in terms I through III is replaced here by the stabilized mean temperature T_0 of the specimen.

Figures 4 a) through 4 c) show the evolution of the three distinct coupling terms for different mean loads at the same load amplitude. Coupling term I depends on the applied load amplitude only and has a single natural frequency of f_L. The additional coupling terms II and III are composed of a component with a natural frequency of $2 \cdot f_L$, depending on the load amplitude, and a component with a natural frequency of f_L, depending on the applied mean load. The superposition of all three terms causes

a) a variation of the temperature changes at f_L with the load amplitude and the mean load
b) a variation of the temperature changes at $2 \cdot f_L$ with the load amplitude

In contrast to plasticity induced variations the temperature signal at $2 \cdot f_L$ is purely harmonic for harmonic loading and thus does not cause the appearance of further harmonics. Even though we could experimentally verify the dependency of the thermoelastic coupling on the mean load level, any further applicability e.g. to investigate residual stresses is questionable, since all effects are small and can hardly be distinguished from natural scatter.

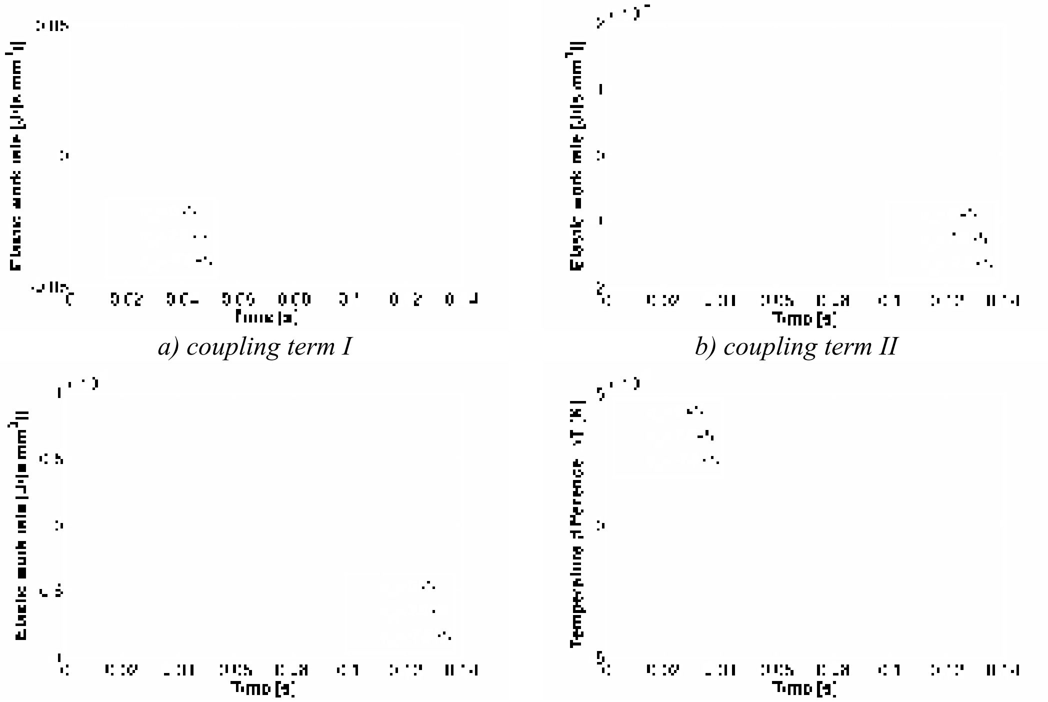

a) coupling term I *b) coupling term II*

c) coupling term III *d) temperature difference*

Figure 4. Temperature difference between elastic-plastic and linear-elastic material behaviour, F_a=var., f_L=15 Hz.

3.4 Influence of bidirectional coupling

The influence of bidirectional coupling can be included in the numerical model if the effect of the temperature changes induced by thermomechanical coupling on the stress or strain state is taken into account. A simple check on the order of magnitude for the given steel demonstrates that the effects of bidirectional coupling are in the range of about 1% of the unidirectional thermomechanical coupling. A short mind-experiment allows one to rationalize the effects of bidirectional coupling: The temperature changes due to thermomechanical coupling are positive during compression and negative during tension. Accordingly they cause a mechanical stress or strain field which acts against the applied mechanical loading. The effect is a stiffening of the specimen with respect to the mechanical loading. Owing to thermoelasticity one would therefore observe an apparent increase of the Young's modulus between isothermal (i.e. slow) and adiabatic (fast) experiments. On the other hand if one measured the coefficient of thermal expansion during the same experiments, the stiffening of the specimen would cause a decrease of the thermal expansion $\alpha = d\varepsilon/dT$ for adiabatic with respect to isothermal experiments. Normally both material parameters are obtained under quasi-isothermal conditions. In this case the coupled approach should be used. For our purposes we evaluated the coefficient of thermal expansion by measuring the thermoelastic temperature changes during mechanical loading under the assumption of a decoupled approach. The Young's modulus has been specified during quasi-static isothermal experiments. In this case the measured coefficient of thermal expansion thus already includes the effects of bidirectional coupling and gives correct results for the temperature changes if the decoupled approach is used.

3.5 Other potential nonlinearities

Another potential nonlinear phenomenon arises if the actual temperature T is used within the thermoelastic coupling terms. A check on the order of magnitude shows that the error made by using the mean temperature T_0 instead of the actual temperature T is negligible for our purposes. Further nonlinearities are caused by the temperature or stress dependency of the material parameters. The influence of the temperature dependency of the Young's modulus has been discussed before. It can be shown that it equals a stress dependency of the coefficient of thermal expansion [7] so that only one of the two effects needs to be taken into account. The order of magnitude of all other dependencies can easily be estimated based on simple calculations or literature data which proofs that these effects are negligible for the given steel. As a result of the numerical investigations it can be concluded that significant nonlinearities in the temperature signal are only caused by plastic dissipation and to a minor degree by the temperature dependency of the Young's modulus. Of course strong nonlinearities arise in the temperature signal due to the presence of cracks (crack closure and opening) or other nonlinearities in the structural behaviour [1]. The analysis of local nonlinearities in the thermomechanical temperature evolution should therefore be an adequate tool to investigate fatigue damage phenomena as cyclic plasticity and/or fatigue crack initiation.

4 EXPERIMENTAL INVESTIGATIONS

In order to investigate the damage evolution during load-controlled fatigue testing experimental studies on specimens with geometries according to figure 1 have been performed in a servohydraulic testing machine (MTS 810, 250 kN). The specimens have been mechanically worked out of a steel plate with a thickness of 20 mm and the material parameters specified in table I. The direction of rolling of the steel-plate coincides with the longitudinal axis of the specimen. The unwelded specimens have been tested under annealed conditions, the welded specimens in the condition as received after manufacturing. During testing the surface temperature distribution of the specimens has been recorded in intervals of 10000 to 30000 load cycles by a high resolution infrared camera (FLIR Phoenix, 640x512 InSb detector). The camera has been used in a subframe-mode which results in an effective frame rate of f_{IR} = 412.5 Hz. At each shot a sequence of about 2000 individual frames showing the temporal variation of the surface temperature were recorded. The only specimen preparation for the thermographic investigations is the application of a fast-drying graphite spray to the investigated specimen side prior to testing in order to increase and equalize the thermal emissivity. All fatigue tests were performed under load-controlled, sinusoidal, fully reversed loading (R = -1) at a loading frequency f_L = 2.5 Hz (cylindrical specimens) or f_L = 15 Hz (notched and welded specimens) with loading acting in the longitudinal direction of the specimens. At the chosen load amplitudes the maximum stresses throughout the entire specimen did not exceed the monotonic yield limit of the steel. The fatigue lifetimes of the specimens varied between 10^5 and $2.0{\cdot}10^6$ load cycles. Data processing is discussed in [6] and is therefore only roughly sketched here. The main idea is the separation of the local linear temperature amplitudes T_a^{lin} due to thermoelasticity and the amplitude of the nonlinearities in the temperature signal T_a^{nlin} due to plasticity, cracks etc. based on a special fitting procedure in the time domain. Some specialized filtering and correction techniques are used to improve the data quality prior to analysis.

4.1 Results on unnotched specimens

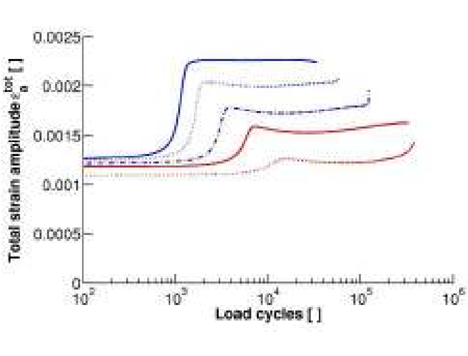

a) evolution of total strain amplitudes

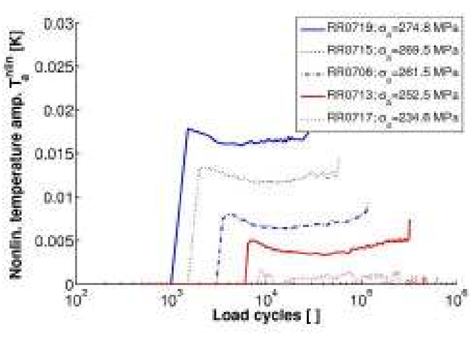

b) evolution of nonlinear temperature amplitudes

Figure 5. Evolution of the total strain amplitudes and the corresponding nonlinear temperature amplitudes in the mid section of the cylindrical specimen, F_a=var., f_L=2.5 Hz.

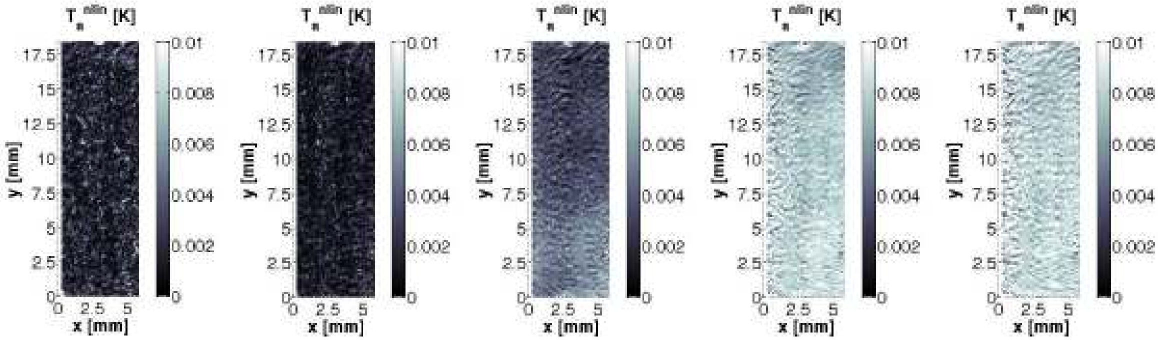

500 load cycles *2500 load cycles* *3000 load cycles* *3500 load cycles* *4000 load cycles*

Figure 6. Spatial evolution of the nonlinear temperature amplitudes in the middle section of the cylindrical specimen during primary softening, σ_a=261.5 MPa., f_L=2.5 Hz.

Figure 5 a) and 5 b) show the evolution of the longitudinal strains in the mid-section of the un-notched specimens during testing and the corresponding evolution of the nonlinear temperature amplitudes. The strains were measured by strain gauges applied to the backside of the specimen. An additional unloaded reference gauge has been used as temperature compensation. The evolution of the strains corresponds to the general softening behaviour of low carbon steels investigated e.g. by [9]. The cyclic behaviour can be roughly distinguished into a linear elastic incubation interval, a phase of primary softening and a phase of more or less stable plastic strains. Figure 5 b) shows the corresponding evolution of the nonlinear temperature amplitudes which closely follows the evolution of the plastic strains. The nonlinearities in the temperature signal become nonzero with the onset of primary softening and similar to the plastic strain quickly reach their maximum after softening. The amplitude of the nonlinearities increases with increasing plastic strain amplitudes which verifies the direct relation to the softening and hardening behaviour. Figure 6 gives the spatial distribution of the nonlinear temperature amplitudes across the mid section of one of the specimens at different load cycle numbers. The results show that the plastic strains evolve in form of cyclic Lueders bands which start at one point of the specimen and spread within hundreds of load cycles. This result corresponds to results obtained by stress-optical methods [2].

4.2 Results on notched specimens

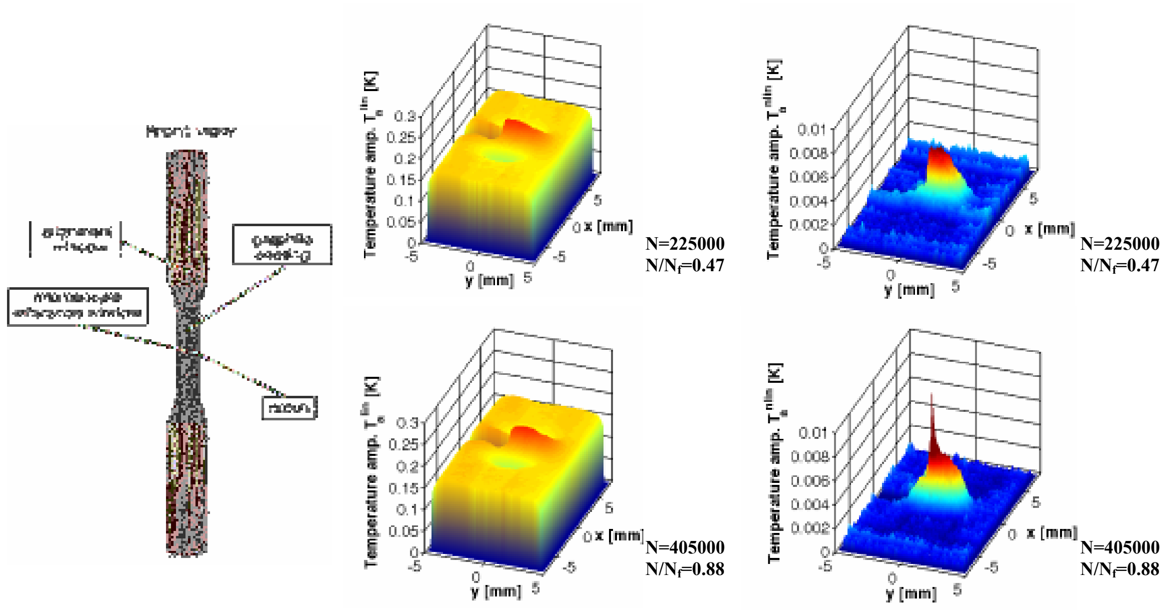

a) linear temperature amplitude *b) nonlinear temperature amplitude*

Figure 7. Distribution of the linear and nonlinear temperature amplitudes on the front surface of the notched specimen type, F_a=18 kN, f_L=15 Hz.

Figure 7 shows the distribution of the linear and nonlinear temperature amplitudes across the surface of the notched specimen type at two different stages of the fatigue testing. Figure 7, upper row, gives the situation after 225000 load cycles. The elevated linear temperature amplitudes in the mid section of the specimen reveal the stress concentrations around the geometric notch. The temperature values of a small area within the notch have been set to zero. In this part of the specimen no graphite coating has been applied to allow for parallel microscopic investigations of the specimen surface. With the chosen load amplitudes only elastic deformations occurred throughout the entire specimen during the first load cycles. After an initial phase the material in the notch starts to soften which is indicated by an increase of the nonlinear temperature amplitudes in the notch area. Compared to the cylindrical specimens the softening process evolves more gradually and requires more load cycles upon complete stabilization. This has been attributed to the complex stress redistributions around the notch with the onset of local plastic deformations. The distribution of the nonlinear temperature amplitudes after 225000 load cycles demonstrates that throughout the entire fatigue test plastic deformations remain bound to the notch area whereas the material within the nominal cross-section still behaves linear-elastic. This finding could also be confirmed by microscopic investigations within the notch and the nominal cross-section of the specimen which revealed concentrated slip band formation throughout the notch bottom. Fatigue crack initiation and growth is indicated by a strong local increase of the nonlinearities (figure 7 b), bottom row) in the temperature evolution which allows to estimate the location and the time of the fatigue crack initiation. Generally we found for the notched specimens that the fatigue cracks initiated around 75% to 85% of the total fatigue lifetime.

4.3 Results on welded specimens

Figure 8 shows the distribution of the linear temperature amplitudes around the front side of one of the welded specimens and the evolution during fatigue testing. The stress concentrations at the weld toe cause increased temperature amplitudes with respect to the nominal cross-section of the specimen. By contrast the temperature amplitudes within the weld bead are strongly reduced. By direct comparison with visual images of the weld we were able to directly locate the most loaded sections of the weld toe. Generally both image types could be directly fused together and the agreement between the visual and the temperature amplitude images was extremely good. From the results in figure 8 the following conclusions can be drawn for the fatigue process: At around 9% of the total fatigue lifetime of the specimen the linear temperature amplitudes at the upper right edge of the weld toe drop locally. This indicates the initiation of a fatigue crack in this section. Additional investigations of marker lines on broken specimens revealed that at this point the cracks are normally relatively wide but only tenth of millimetres deep. During further testing the fatigue cracks grow along the width of the weld toe. At 40% of the fatigue lifetime further fatigue cracks initiate in the middle section of the second weld toe. In both weld toes the fatigue cracks grow until final failure of the specimen. Parallel visual inspection of the specimens failed to reveal the fatigue cracking until final rupture. For all specimens the initiation of the fatigue cracks was first indicated by a local drop of the linear temperature amplitudes and shortly afterwards by a rise of the nonlinear temperature amplitudes (not shown here). For none of the specimens any indication on the existence of local elastic-plastic cyclic material behaviour prior to crack initiation could be found. Generally the first cracks could be observed around 10 to 20% of the total fatigue lifetime. The results demonstrate that by contrast to the un-notched or mildly notched specimens crack propagation is the dominant process for the fatigue behaviour of the weld seam.

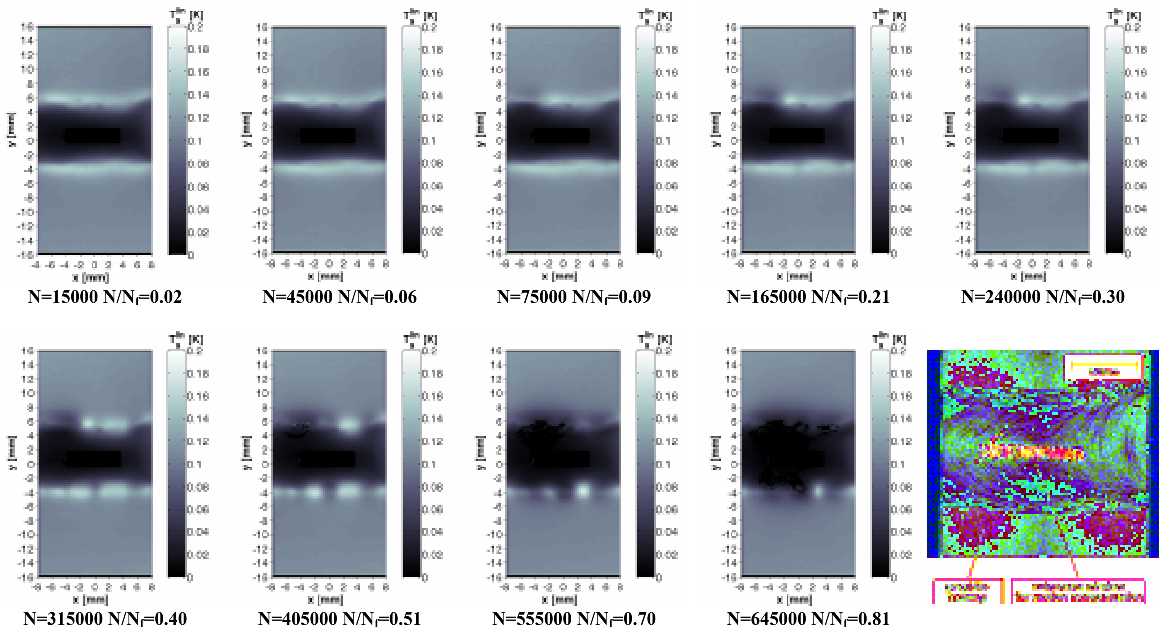

Figure 8. Evolution of the linear temperature amplitude on the front surface of a welded specimen with respect to the applied load cycles, F_a=17.5 kN, f_L=15 Hz.

5 CONCLUSION

An experimental approach for the in-situ analysis of fatigue processes during fatigue testing has been proposed. The methodology is based on infrared thermographic investigations during fatigue loading. By contrast to former approaches only the short term temperature evolution due to thermomechanical coupling is considered and analysed with respect to damage processes. Based on numerical investigations we could verify that for the used mild steel the only relevant nonlinearities in the temperature evolution are caused by cyclic plasticity and fatigue cracks. Therefore the extraction of the nonlinearities in the temperature evolution allows for investigations of local damage processes. For this purpose a specialized data processing technique is used which allows for the retrieval of temperature amplitudes as small as 1 to 2 mK. This is sufficient to investigate the local cyclic softening and hardening behaviour as well as the early formation and propagation of fatigue cracks. The new method has been successfully applied during fatigue testing on different specimen geometries and gives qualitative insight in the local fatigue damage accumulation. Further work concentrates on an improved quantification of the results.

6 ACKNOWLEDGEMENTS

The authors would like to thank the German Research Foundation DFG for the funding of these studies within the framework of the collaborative research centre SFB 477 at the Technical University Carolo-Wilhelmina Braunschweig/Germany.

7 REFERENCES

1. A. Huss, Rissdetektion und -bewertung mit dem Verfahren der thermoelastischen Spannungsanalyse, VDI - Fortschritt Berichte, Vol. 18 No.147, 1994.
2. D.P. Gonzales, Zum Wechselverformungsverhalten normalisierter unlegierter Staehle mit Kohlenstoff-gehalten von 0,01 bis 1,02 GEW %, PhD thesis, Universitaet Karlsruhe, 1979.
3. J. Lemaitre and J.-L. Chaboche, Mechanics of solid materials, Cambridge University Press, Cambridge, 1990.
4. M.P. Luong, Workshop Optimal Design, Palaiseau, November 26-28, 2003.
5. A.S. Machin, J.G. Sparrow, M-G. Stimson, *Strain*, 23, 1987, 27-29.
6. J. Medgenberg, T.Ummenhofer, Thermosense XXIX, Orlando, April 9-12, K. M. Knettel, V.P. Vavilov, J.J. Miles, Ed., Proc. of SPIE -Volume 6541, 2007.
7. G. Pittaresi, E.A. Patterson, *J. Strain Analysis*, 38(5), 2003, pp. 405-417
8. T. Ummenhofer and J. Medgenberg, *QIRT Journal* 3 (1), 2006, pp. 71-93.
9. M. Weber, Untersuchungen zum zyklischen Verformungsverhalten von Stahl. PhD thesis, Universitaet Gesamthochschule Essen, Essen, 1983.
10. A.K. Wong, J.G. Sparrow, S.A. Dunn, *J. Phys. Chem. Solids*. 48(8), 1987, pp. 749-753